Abstract

A set of *Hox* genes expressed during embryonic process presents a crucial system to set up the body plan in animal phyla. Current systematic approaches, such as bio-imaging, epigenetic regulation and phylogenetic genome comparison, illuminated new comprehensive insights into *Hox* genes as an evolutionary constraint for vertebrate body plan, which provides a novel counter-view to give further insights into the evolution and development of the craniofacial and dental systems as non-Hox systems.

Key Words,

embryogenesis, evolution, genome

Introduction

One of characteristic features of the vertebral body is the anatomical repetitions along its axis, as seen in the axial skeleton (vertebrae), their associated muscles and nervous systems [1]. This repetitive pattern is imposed by an embryonic segmental structure; the somite (Figure 1, A). Vertebrate somites are mesoderm-derived epithelial blocks that contain the precursors of vertebrae, skeletal muscles and other connective tissues. Even though each somite shows a very similar epithelial cubic structure when formed, it eventually differentiates into the distinct morphology of its derivatives depending on its position along anterior-posterior body axis, which is represented by the distinct morphology of each vertebral element. The morphological identities of somite derivatives are largely governed by *Hox* genes [2,3,4,5](Figure 1). This short review will briefly overview current topics in *Hox* genes that constitute an evolutional constraint of global body patterning, which appear to make a striking contrast to craniofacial and dental systems that have

been proposed to be facilitated by functional diversity and plasticity among the participating tissues during vertebrate evolution.

Hox genes; temporal collinearity and spatial collinearity

Vertebrate embryos develop in a similar progressive fashion in which anterior structures are formed first, and then more posterior structures are progressively produced by gastrulation following the primitive streak and tail bud regression (Figure 1). Therefore, the position of these structures along the anterior-posterior (AP) axis in an embryo directly reflects the timing of their production. This mode of body axis formation is highly invariable among vertebrates, suggesting an evolutionary constraint in which the temporal control of tissue formation and spatial regionalization along the AP axis must be highly coordinated during embryonic development. Although morphologically very similar, somites will differentiate into morphologically distinct vertebrae depending on their axial level which ultimately defines the axial formula (e.g. the occipital, cervical, thoracic, lumbar, sacral and caudal spine). This positional identity of somites is specified largely by their unique combinatorial expression of *Hox* genes in the somitic mesoderm [6](Figure 1, C). Mammals have 39 *Hox* genes that are organized into four clusters. Birds are believed to have the same set of Hox clusters, though the chicken genome has not yet been perfectly annotated. The genes in each cluster are arranged on the chromosome in a sequence that reflects both the chronological and spatial orders of their expression during embryogenesis (Figure 1, B-C). The former correlation has been described as 'temporal collinearity' while the latter has been described as 'spatial collinearity' [7,8,9]. As described above, the vertebrate body axis progressively extends in a posterior fashion when new tissues are added from the gastrulation site at its posterior end. *Hox* clusters initiate their activity in gastrulating cells in a collinear manner in which 3′ *Hox* genes are expressed first, and then later, more 5′ *Hox* genes become progressively activated during axis elongation. The collinear activation

of *Hox* genes in gastrulating cells coupled with the mode of body axis elongation results in cells being produced earlier to express more 3 *Hox* genes and being located more anterior structure. This correlation led to the idea that the spatial expression of *Hox* genes along the AP axis is merely the readout of the progressive mode of axis extension in vertebrates (Figure 1, B-C). A significant amount of evidence supports th functional relevance of initial expression of *Hox* genes in early embryogenesis to establish the positional identities of somitic derivatives.

Relevance of early *Hox* gene expression for morphological identity of somite derivatives

Chick transplantations and mouse genetic experiments have led to the idea that *Hox* gene expression is correlated to the acquisition of future somite identity as early as the unsegmented PSM stage. After heterochronic transplantations of embryonic spine precurors: the paraxial mesoderm (PSM), grafted cells still maintain their original *Hox* gene expression and tend to differentiate according to their original identity even when placed at a distinct axial level in the host [10,11,12]. The relevance of the precise temporal activation of *Hox* genes is also supported by mutations of *Hox* early enhancers in the mouse. These mutations, which cause an initial delay of a given *Hox* gene expression, affects skeletal patterning by largely phenocopying the null mutant of the same *Hox* even if spatial somitic expression appears to be recovered at later stages[13,14,15]. Therefore, the activation of *Hox* genes at an early stage of paraxial mesoderm development plays a crucial in establishing regional identity. Furthermore, overexpression of *Hox* genes driven by a PSM-specific promoter demonstrates a severe effect on skeletal patterning; whereas, the overexpression from a promoter driving expression in somites does not elicit such phenotypes[16].

Mode of mesoderm formation and initial function of Hox genes

Hox genes regulate the timing of mesoderm formation through controlling the flux of epiblast cells to the primitive streak which could provide the initial regulation of functional *Hox* expression for the morphological identity[17]. This is an unique mechanism to achieve regionalization during embryonic body formation. Detailed fate mapping of the epiblast and careful observation of *Hoxb* gene initiation in the chick embryo demonstrate that *Hoxb* gene transcription is sequentially initiated in the epiblast at the level of the middle-to-posterior streak, which gives rise to mainly lateral plate and extraembryonic mesoderm[17]. Subsequently, the expression domain spreads anteriorly through the paraxial mesoderm territory to reach the level of Hensen's node and the posterior neural plate. A similar initiation pattern is observed in the Xenopus marginal zone and the mouse epiblast[2,8,18,19].

Current veiws of the mode of mesoderm formation suggests topological conservation in mode of mesoderm formation among vertebrates in which mesodermal precursors sequentially ingress (or involute) into the gastrulation point[20,21,22].

Therefore, the dynamic expression of *Hox* genes follows the gastrulation movements of cells from the epiblast to the mesoderm, suggesting that *Hox* genes could play a role in mesoderm formation through gastrulation. This hypothesis was tested by electroporation of Hox-expression constructs containing a fluorescent reporter. The overexpression of *Hoxb* genes in chick embryos in the presumptive territory of the somites in the epiblast at the gastrula stage resulted in collinear phenotypes in terms of AP distribution of Hox-expressing cells. Cells overexpressing more anterior *Hox* genes contributed to more anterior portions of the somitic column, whereas cells overexpressing more posterior *Hox* genes contributed to more caudal domains. Overexpression of posterior *Hox* genes (e.g. Hoxb7 or Hoxb9) causes the *Hox* expressing cells to stay in the epiblast longer than cells expressing either control GFP or anterior *Hox* genes (e.g. Hoxb1 and Hoxb4). A

deletion mutant of the third helix of Hoxb9 homeodomain does not show this delayed effect on epiblast ingression, suggesting that DNA binding is essential for this function. Therefore, the sequential activation of *Hox* genes controls the timing of cell ingression to the primitive streak, therefore regulating the AP distribution of mesodermal cells. This function of Hox genes on mesodermal cell distribution along the AP axis conjugated with their temporal collinear activation most likely provides the initial information in establishing the spatial collinearity, and could therefore provide a framework to elucidate the diversification of the axis formula among vertebrate species[5].

Genomic structures and collinear transcriptional regulation

A functional link between the tight collinear arrangement of *Hox* genes in the genome and the temporal collinear activation during embryogenesis has been postulated for vertebrates[3,4,5,23]. Genomic relocations of *Hoxd/LacZ* transgenes at distinct positions in the *Hoxd* cluster identified a global regulatory element in the 5end of the *Hoxd* complex[14,15,24]. This element is essential for the early collinear activation of the cluster. Together, these observations suggest a silencing mechanism originating at the 5′end of the cluster, which sequentially makes genes available for transcription in a 3′to 5′order (Figure 2, B-C).

***Hox* function on the axial formula**

A conserved feature of the vertebrate axis is the order of morphologically distinct regions along the AP axis level (e.g. cervical, thoracic, lumbar, sacral and caudal vertebrae). Yet, different numbers of segments contribute to various regions resulting in the variation of axial formulae between

vertebrate species. These morphological transpositions are paralleled by corresponding transpositions of the *Hox* gene anterior expression boundaries, suggesting an evolutionally conserved role of *Hox* genes in the positioning of vertebral domains rather than in the specification of each segment[25]. This observation suggests a conserved qualitative function of *Hox* paralogues on defining an embryonic area.

Posterior prevalence, rather than "Hox code"

The idea that the most posterior genes expressed in a particular embryonic domain impose their dominant function on more anterior genes is described as the posterior prevalence or phenotypic suppression of *Hox* genes[26,27] (Figure 2, C). In many cases, the posterior prevalence concept accounts for phenotypes of *Hox* mutants in a better way than the Hox code concept in which a combinatorial distribution of Hox products leads to morphological diversity of an individual vertebra[6]. The Hox code hypothesis proposes that changes in the combinatorial outputs would impose phenotypes in the whole expression domain of these mutated genes. However, actual phenotypes in null mutants for all the paralogues in a group are restricted to the narrow window of the anterior expression domain of these paralogues[28,29,30]; whereas, the posterior domain overlapped by more posterior *Hox* genes shows intact morphology, which must therefore be imposed by the posterior genes. Molecular mechanisms underlying the posterior prevalence remain unclear. The possible involvement of posttranslational regulation and miRNA rather than direct transcriptional repression has been discussed[4].

Collinear *Hox* system from phylogenetic views

A recent comparison of the genomic structures of the *Hox* gene in various animal species has challenged the conventional view of the *Hox* gene and its evolution[23] (Figure 2, A). This intensive insight indicates that *Hox* genes are encoded in a same strand and arranged in a tandem manner without any insertion by other gene, but only in vertebrates that have the best organized Hox clusters (type O) spanning ~100Kb. In marked contrast, many other animal groups have more disorganized (type D), split (type S) or even atomized (type A) *Hox* cluster. Type D has longer genome size and mixed-up genes with the opposite direction being interspaced by non-*Hox* genes, whereas type S has split clusters of type O or D features, and type A has lost its "cluster" structure with genes located separately in distinct genome loci. Type D examples are found in sea urchin and a cephalochordate, amphioxus. Type S and A are exemplified by *Drosophila* and *Olikopleura* respectively. This phylogenetic comparison predicts that the ancestral cluster would be type D, indicating type O would have been evolved only along the vertebrate lineage. On the other hand, type D would have evolved into type S and A along other lineages, implicating that the evolution of *Hox* gene cluster may not have proceeded simply by the progressive expansion and diversification of the genes. Therefore, it would be only vertebrates that have evolved the functional link between the tight collinear arrangement of *Hox* genes in the genome and the temporal collinear activation during embryogenesis (Figure 2). In other words, global regulatory enhancers and associated spatio-temporal regulations of a *Hox* cluster, by which a single compacted cluster is activated as a single transcriptional unit rather than a cluster of multiple genes with distinct transcriptional regulations, has been selected only for vertebrate body plan. Consistently, human genome sequencing demonstrates the extremely low density of interspersed repeats (as *Alu* sequence) in the four *HOX* clusters, suggesting that large- and short-scale *cis*-regulatory elements in each cluster are a strong selective constraint that cannot tolerate being interrupted by insertions[31].

Visualization of transcriptional control by nuclear organization

The sequential activation of the genes along the *Hoxb* cluster was observeded in mouse embryonic stem (ES) cells[32] and in early mouse embryos[33] by fluorescent *in situ* hybridization (Figure 2, C). The short exposure of ES cells to RA at a time when only *Hoxb1* is activated is sufficient to induce a general decondensation of the *Hoxb* locus and selectively induce *Hoxb1* looping out of its chromosome territory (CT), while *Hoxb9* is neither expressed nor looped out. Longer RA incubation, however, induces both *Hoxb1* and *Hoxb9* looping out of the CT. In gastrulating embryos, looping out of *Hoxb1* from the CT was observed where *Hoxb1* was first expressed. In the tail bud of an E9.5 embryo where both genes are expressed, both *Hoxb1* and *Hoxb9* looped out of the CT. These observations demonstrate that chromatin decondensation and successive looping out of the CT is tightly concomitant with gene transcription in both *in vitro* and *in vivo* contexts. Although a functional link between the looping out of genes and transcription remains to be established, the extrusion of a locus from the CT probably represents a poised state for transcription.

Conclusion remarks,

Vertebrates have invented a highly elaborated body patterning system with genomic organization of Hox clusters, which does not appear to be explained by mere genomic expansion and diversification. the craniofacial and dental system is developed from the anterior most embryonic region that is in "*Hox* default" status, it is intrigue to consider how discontinuation or renunciation of the Hox system have contributed to evolution and development of the maxillofacial system[34,35]. More

integrative models or conceptual frameworks are therefore necessary to assess the total patterning of the body plan.

Acknowledgements

We would like to express sincere thanks to Professor Hidenori Ichijo and Assoicaite Professor Kohsuke Takeda (The University of Tokyo, Graduate School of Pharmaceutical Sciences) for giving an opportunity to give a talk on this subject in the 51st Annual Meeting of the Japanese association for Oral Biology held in Niigata City, and to Professor Hayato Ohshima (Niigata University, Graduate School of Medical and Dental Sciences) for the invitation to write this review paper. The current work was supported by the grant from the Japanese Ministry of Education, Global Center of Excellence (GCOE) Program, "International Research Center for Molecular Science in Tooth and Bone Diseases". T. I. was also supported by the Takeda Science Foundation, the Mochida Memorial Foundation for Medical and Pharmaceutical Research and a Grant-in-Aid for Scientific Research from the Japan Society for the Promotion of Science (21659426).

Figure Legends

Figure 1

A) A schematized view of vertebrate body formation. The progressive mode of mesodermal segmentation (somitogenesis) follows body axis elongation. Molecular controls of morphogenesis by *Hox* genes and the segmentation clock are initiated at the growth zone known as the primitive streak or tail bud that is located at the tip of an embryo. Tissue

differentiation into skeletal elements, muscle and other connective tissues are specified in formed somites by neighboring embryonic tissues.

B) The schematized structure of a Hox cluster. In this scheme, four *Hox* genes are arranged in a tandem manner from the 3' to 5' direction on a chromosomal region. The order of *Hox* genes along a genome DNA correlates their temporal and spatial expression (spatial collinearity and temporal collinearity).

C) The establishment of *Hox* expression domains in an ideal scheme. In the youngest embryo (Stage-1), the first *Hox* gene (named Hox1 and marked in red) is initiated in the growth zone. In the next stage (Stage-2), *Hox-1* positive cells are colonized into anterior most mesoderm and some of them are already incorporated into somites, whereas the second *Hox* gene (named *Hox2* and marked in yellow) begins to express in the growth zone. In the following stages (Stage-3 and -4), *Hox* genes located more 5' regions (*Hox3* and *Hox4* and marked in green and blue, respectively) are progressively activated one by one in the progressive zone. Therefore, progressive modes of *Hox* activation and body axis elongation cooperatively endow spatial nested expression patterns of *Hox* genes, which is often described as "Translation of the spatial collinearity into the temporal collinearity". Note that the colors in a body column indicate a functional *Hox* gene at a given body axis level, since the largest numbered *Hox* gene is functionally dominant over the other *Hox* genes expressed in that region, which is known as "Posoterior prevalence of *Hox* genes". For instance, in the green region, *Hox3* is functionally dominant though *Hox1* and *Hox2* are concomitantly expressed in this region (see the nest expression pattern).

Figure 2

A) Structural classification of *Hox* clusters[23]. The type O (organized) cluster is well organized with no insertion of foreign genes ~100 Kb in genome size and all the *Hox* genes (black boxes) are transcribed in the same direction, which represents vertebrate clusters. Type D (disorganized) cluster is much larger in size (~10 times as large as the type O), and contains Hox genes in opposite orientations and several non-*Hox* genes (white boxes). Type D examples are found in amphioxus and in sea urchins. Split (type S) cluster appears to be tore into a couple of sub-clusters, in each of which has Type O or Type D features. The drosophila *HOM* complex represents this Type S cluster. Type A (atomized)'cluster' represents the 'no-cluster' situation, in which *Hox* genes are found to be scattered in various genomic loci. The type A cluster is found in Oikopleura.

B) Global control region (GCR) and local *cis*-regulatory region(s) control *Hox* transcription. Type O *Hox* cluster mainly evolved in vertebrates may have facilitated GCR-derived transcriptional control of a *Hox* cluster, which probably governs the sequential activation of *Hox* genes in the cluster through long-range *cis*-regulation. The GCR control could involve 'regulatory priming' that intrinsically release a *Hox* locus and make it progressively accessible to transcriptional machinery as shown in (C). Local *cis*-regulatory region between *Hox* genes controls adjacent genes, which could have been operated in Type D and S clusters.

C) Time-based activation of a *Hox* cluster through progressive chromatin remodeling. During the course of embryonic development, changes in chromatin configuration allow

Hox genes that are initially silenced to become progressively accessible to achieve transcriptional regulation.

1 Hirsinger, E., Jouve, C., Dubrulle, J. & Pourquie, O. Somite formation and patterning. *Int Rev Cytol* **198**, 1-65 (2000).

2 Deschamps, J. & van Nes, J. Developmental regulation of the Hox genes during axial morphogenesis in the mouse. *Development* **132**, 2931-2942,(2005).

3 Kmita, M. & Duboule, D. Organizing axes in time and space; 25 years of colinear tinkering. *Science* **301**, 331-333, (2003).

4 Iimura, T., Denans, N. & Pourquie, O. Establishment of Hox vertebral identities in the embryonic spine precursors. *Curr Top Dev Biol* **88**, 201-234, (2009).

5 Iimura, T. & Pourquie, O. Hox genes in time and space during vertebrate body formation. *Dev Growth Differ* **49**, 265-275, (2007).

6 Kessel, M. & Gruss, P. Homeotic transformations of murine vertebrae and concomitant alteration of Hox codes induced by retinoic acid. *Cell* **67**, 89-104, (1991).

7 Dolle, P., Izpisua-Belmonte, J. C., Falkenstein, H., Renucci, A. & Duboule, D. Coordinate expression of the murine Hox-5 complex homoeobox-containing genes during limb pattern formation. *Nature* **342**, 767-772, (1989).

8 Gaunt, S. J., Sharpe, P. T., and Duboule, D. Spatially restricted domains of homeogene transcripts in mouse embryos: Relation to a segmented body plan. *Development* **104**, 169–179 (1988).

9 Graham, A., Papalopulu, N. & Krumlauf, R. The murine and Drosophila homeobox gene complexes have common features of organization and expression. *Cell* **57**, 367-378, (1989).

10 Kieny, M., Mauger, A. & Sengel, P. Early regionalization of somitic mesoderm as studied by the development of axial skeleton of the chick embryo. *Dev Biol* **28**, 142-161 (1972).

11 Nowicki, J. L. & Burke, A. C. Hox genes and morphological identity: axial versus lateral patterning in the vertebrate mesoderm. *Development* **127**, 4265-4275 (2000).

12 Jacob, M., Christ, B. & Jacob, H. J. [Regional determination of the paraxial mesoderm in young chick embryos]. *Verh Anat Ges* **69**, 263-269 (1975).

13 Juan, A. H. & Ruddle, F. H. Enhancer timing of Hox gene expression: deletion of the endogenous Hoxc8 early enhancer. *Development* **130**, 4823-4834, (2003).

14 Kondo, T. & Duboule, D. Breaking colinearity in the mouse HoxD complex. *Cell* **97**, 407-417, (1999).

15 van der Hoeven, F., Zakany, J. & Duboule, D. Gene transpositions in the HoxD complex reveal a hierarchy of regulatory controls. *Cell* **85**, 1025-1035, (1996).

16 Carapuco, M., Novoa, A., Bobola, N. & Mallo, M. Hox genes specify vertebral types in the presomitic mesoderm. *Genes Dev* **19**, 2116-2121, (2005).

17 Iimura, T. & Pourquie, O. Collinear activation of Hoxb genes during gastrulation is linked to mesoderm cell ingression. *Nature* **442**, 568-571, (2006).

18 Deschamps, J. *et al.* Initiation, establishment and maintenance of Hox gene expression patterns in the mouse. *Int J Dev Biol* **43**, 635-650 (1999).

19 Wacker, S. A., Jansen, H. J., McNulty, C. L., Houtzager, E. & Durston, A. J. Timed interactions between the Hox expressing non-organiser mesoderm and the Spemann organiser generate positional information during vertebrate gastrulation. *Dev Biol* **268**, 207-219, (2004).

20 Iimura, T., Yang, X., Weijer, C. J. & Pourquie, O. Dual mode of paraxial mesoderm formation during chick gastrulation. *Proc Natl Acad Sci U S A* **104**, 2744-2749, (2007).

21 Solnica-Krezel, L. Conserved patterns of cell movements during vertebrate gastrulation. *Curr Biol* **15**, (2005).

22 Cambray, N. & Wilson, V. Two distinct sources for a population of maturing axial progenitors. *Development* **134**, (2007).

23 Duboule, D. The rise and fall of Hox gene clusters. *Development* **134**, 2549-2560, doi:dev. (2007).

24 Kondo, T., Zakany, J. & Duboule, D. Control of colinearity in AbdB genes of the mouse HoxD complex. *Mol Cell* **1**, 289-300, (1998).

25 Burke, A. C., Nelson, C. E., Morgan, B. A. & Tabin, C. Hox genes and the evolution of vertebrate axial morphology. *Development* **121**, 333-346 (1995).

26 Duboule, D. & Morata, G. Colinearity and functional hierarchy among genes of the homeotic complexes. *Trends Genet* **10**, 358-364 (1994).

27 Duboule, D. Patterning in the vertebrate limb. *Curr Opin Genet Dev* **1**, 211-216 (1991).

28 Horan, G. S. *et al.* Compound mutants for the paralogous hoxa-4, hoxb-4, and hoxd-4 genes show more complete homeotic transformations and a dose-dependent increase in the number of vertebrae transformed. *Genes Dev* **9**, 1667-1677 (1995).

29 van den Akker, E. *et al.* Axial skeletal patterning in mice lacking all paralogous group 8 Hox genes. *Development* **128**, 1911-1921 (2001).

30 Wellik, D. M. & Capecchi, M. R. Hox10 and Hox11 genes are required to globally pattern the mammalian skeleton. *Science* **301**, 363-367, (2003).

31 Lander, E. S. *et al.* Initial sequencing and analysis of the human genome. *Nature* **409**, 860-921, (2001).

32 Chambeyron, S. & Bickmore, W. A. Chromatin decondensation and nuclear reorganization of the HoxB locus upon induction of transcription. *Genes Dev* **18**, 1119-1130, (2004).

33 Chambeyron, S., Da Silva, N. R., Lawson, K. A. & Bickmore, W. A. Nuclear re-organisation of the Hoxb complex during mouse embryonic development. *Development* **132**, 2215-2223, (2005).

[34] Kuratani, S., Matsuo, I. & Aizawa, S. Developmental patterning and evolution of the mammalian viscerocranium: genetic insights into comparative morphology. *Dev Dyn* **209**, 139-155, (1997).

[35] Stern, C. D. Evolution of the mechanisms that establish the embryonic axes. *Curr Opin Genet Dev* **16**, 413-418, (2006).

Desired sizes of all the figures(Figure1 and 2)will be fitted to a double column.

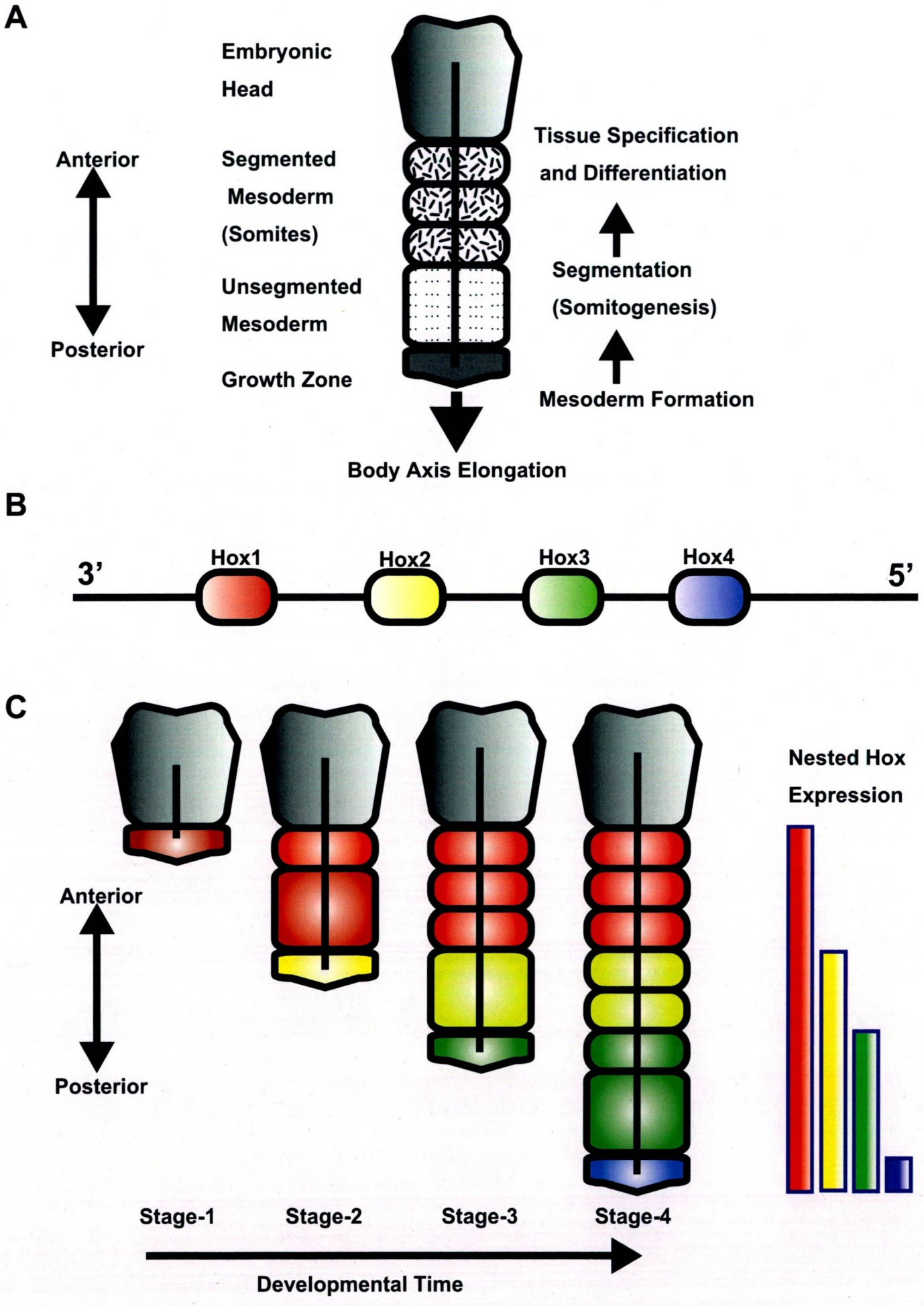

Figure 1, Iimura et al.

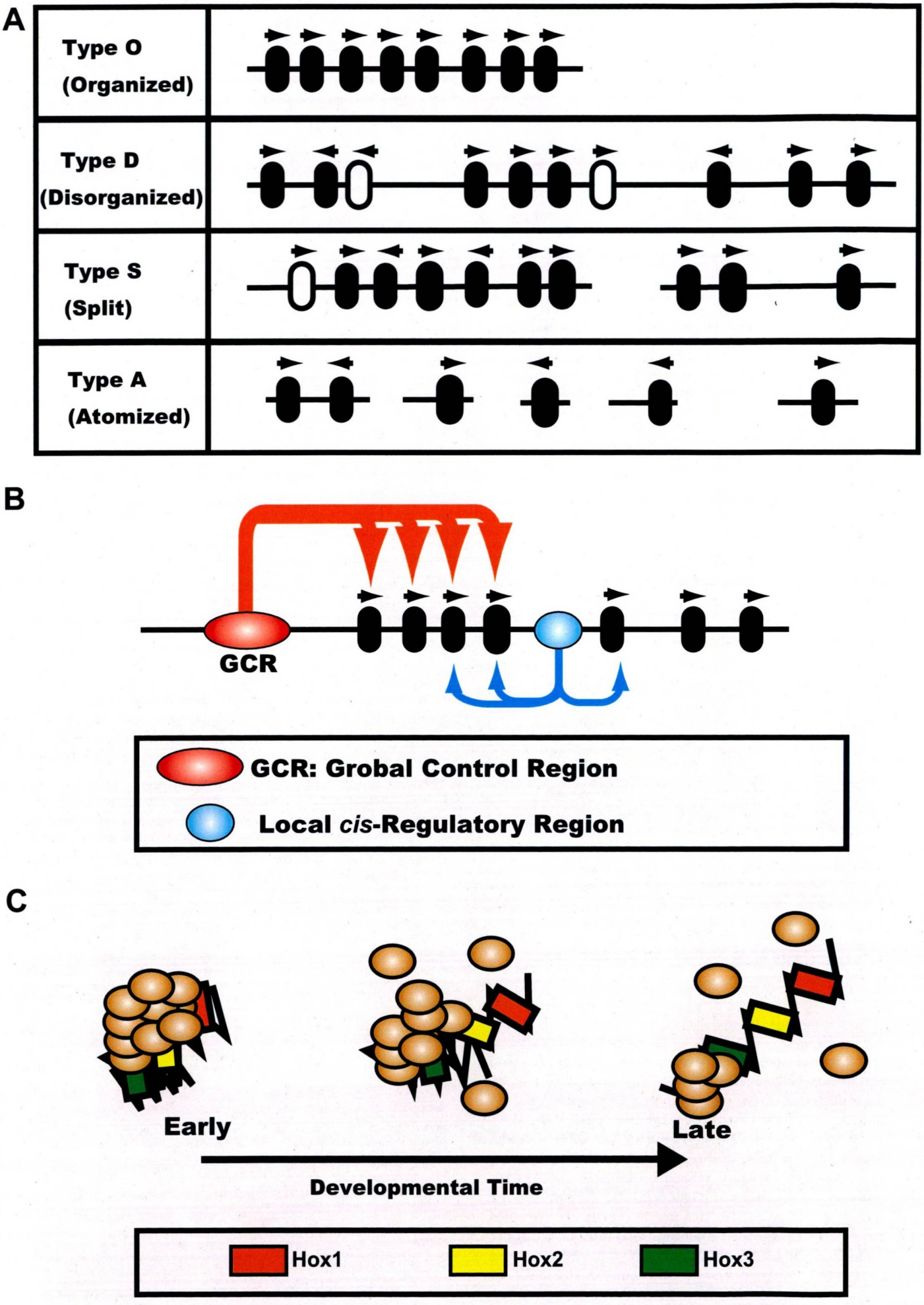

Figure 2, Iimura et al.

The American Journal of Pathology, Vol. 176, No. 2, February 2010

DOI: 10.2353/ajpath.2010.090299

Tumorigenesis and Neoplastic Progression

Roles of Interleukin-6 and Parathyroid Hormone-Related Peptide in Osteoclast Formation Associated with Oral Cancers

Significance of Interleukin-6 Synthesized by Stromal Cells in Response to Cancer Cells

Kou Kayamori,[*†] Kei Sakamoto,[*] Tomoki Nakashima,[‡] Hiroshi Takayanagi,[†‡] Kei-ichi Morita,[§] Ken Omura,[†§] Su Tien Nguyen,[¶] Yoshio Miki,[†¶‖] Tadahiro Iimura,[*†] Akiko Himeno,[*†**] Takumi Akashi,[††] Hisafumi Yamada-Okabe,[‡‡] Etsuro Ogata,[§§¶¶] and Akira Yamaguchi[*†]

From the Sections of Oral Pathology,[*] Cell Signaling,[‡] Oral and Maxillofacial Surgery,[§] and Periodontology,[**] Graduate School of Tokyo Medical and Dental University, Tokyo, the Global Center of Excellence Program,[†] International Research Center for Molecular Science in Tooth and Bone Diseases, and the Departments of Molecular Genetics,[¶] Medical Research Institute, and Pathology,[††] Tokyo Medical and Dental University Medical Hospital, Tokyo, the Department of Genetic Diagnosis,[‖] Cancer Institute, Japanese Foundation for Cancer Research, Tokyo, Pharmaceutical Research Department III,[‡‡] Kamakura Laboratories, Chugai Pharmaceutical Co., Ltd, Kanagawa; Chugai Pharmaceutical Co., Ltd.,[§§] Tokyo, and Cancer Institute Hospital,[¶¶] Tokyo, Japan

We investigated the roles of interleukin-6 (IL-6) and parathyroid hormone-related peptide (PTHrP) in oral squamous cell carcinoma (OSCC)-induced osteoclast formation. Microarray analyses performed on 43 human OSCC specimens revealed that many of the specimens overexpressed *PTHrP* mRNA, but a few overexpressed *IL-6* mRNA. Immunohistochemical analysis revealed that IL-6 was expressed not only in cancer cells but also in fibroblasts and osteoclasts at the tumor-bone interface. Many of the IL-6-positive cells coexpressed vimentin. Conditioned medium (CM) derived from the culture of oral cancer cell lines (BHY, Ca9-22, HSC3, and HO1-u-1) stimulated *Rankl* expression in stromal cells and osteoclast formation. Antibodies against both human PTHrP and mouse IL-6 receptor suppressed *Rankl* in ST2 cells and osteoclast formation induced by CM from BHY and Ca9-22, although the inhibitory effects of IL6 antibody were greater than those of PTHrP antibody. CM derived from all of the OSCC cell lines effectively induced IL-6 expression in stromal cells, and the induction was partially blocked by anti-PTHrP antibody. Xenografts of HSC3 cells onto the periosteal region of the parietal bone in athymic mice presented histology and expression profiles of RANKL and IL-6 similar to those observed in bone-invasive human OSCC specimens. These results indicate that OSCC provides a suitable microenvironment for osteoclast formation not only by producing IL-6 and PTHrP but also by stimulating stromal cells to synthesize IL-6. *(Am J Pathol 2010, 176:968–980; DOI: 10.2353/ajpath.2010.090299)*

Bone invasion by various malignant tumors causes diverse complications in patients. In the case of oral cancers, such invasion leads to physical damage of the bone and has a critical influence on patient prognosis. Several research groups have histopathologically investigated the process of bone destruction by oral squamous cell

Supported by a Grant-in-Aid for Scientific Research from the Japan Society for the Promotion of Science (14104015 to A.Y.) and by a grant from the Japanese Ministry of Education, Global Center of Excellence Program, "International Research Center for Molecular Science in Tooth and Bone Diseases."

Accepted for publication October 15, 2009.

Supplemental material for this article can be found on *http://ajp.amjpathol.org*.

Address reprint requests to Akira Yamaguchi, D.D.S., Ph.D., Section of Oral Pathology, Graduate School of Tokyo Medical and Dental University, 1-5-45 Yushima, Bunkyo-ku, Tokyo 113-8549, Japan. E-mail: akira.mpa@tmd.ac.jp.

carcinoma (OSCC),[1–4] the dominant cancer occurring in the oral cavity. Although these studies indicated that the bone destruction is mediated by osteoclasts rather than directly by cancer cells, the precise mechanism that regulates bone destruction due to OSCC has not been elucidated.

Osteoclastogenesis is regulated by a complex signaling system that involves three essential molecules of the tumor necrosis factor family, namely the receptor activator of nuclear factor-κB (RANK), the RANK ligand (RANKL), and osteoprotegerin.[5,6] RANKL is expressed in osteoblasts and bone marrow stromal cells.[7] It critically regulates the differentiation and function of osteoclasts by binding to its receptor RANK,[8,9] which is expressed in osteoclast lineage cells. Furthermore, osteoblasts and stromal cells synthesize osteoprotegerin,[10] which is a decoy receptor for RANKL. Thus, a balance between the expression levels of RANKL and osteoprotegerin is crucial for regulating osteoclast differentiation and function.

To explore the factors that contribute to cancer-associated bone resorption, several research groups have investigated the expression of bone-resorbing factors such as interleukin (IL)-1β, IL-6, tumor necrosis factor-α, and parathyroid hormone-related peptide (PTHrP) in human OSCC.[11–14] Among these, IL-6 is an important cytokine that stimulates osteoclastic bone resorption by inducing RANKL expression in osteoblastic cells.[15] More importantly, several reports have revealed that the serum levels of IL-6 are elevated in patients with head and neck squamous cell carcinoma (SCC).[16–18] Duffy et al[18] reported that elevated serum IL-6 levels could serve as a valuable biomarker for predicting tumor recurrence and survival among patients with head and neck SCC. Although the increased serum IL-6 is considered to be synthesized by OSCC, this has not been well elucidated. PTHrP, which was originally identified as a factor responsible for humoral hypercalcemia of malignancy,[19] is synthesized by many malignant tumors such as those in breast, lung, colon, and prostate gland.[20–23] PTHrP expression in OSCCs also has been investigated.[24–27] Because PTHrP stimulates osteoclast activity by inducing RANKL in osteoblastic cells,[28] it might play a key role in cancer-associated bone resorption. Although previous reports have suggested the importance of IL-6 and PTHrP in OSCC-induced bone resorption, few studies have investigated extensively the roles in osteoclast formation associated with OSCC.

Cancer stroma comprises various types of cells including fibroblasts, myofibroblasts, endothelial cells, and inflammatory cells. These cells and their products play crucial roles in establishing the tumor microenvironment, which regulates the proliferation, survival, invasion, and metastasis of the cancer cells.[29,30] We investigated histopathologically 97 cases of OSCCs with bone invasion and demonstrated the significant role of fibrous stroma in bone invasion.[31] In all of the cases, we found that the fibrous stroma intervened between the invading cancer nests and the resorbing bone surface, and fibroblastic cells expressing RANKL were observed at the bone resorbing region close to the cancer nests, suggesting that OSCCs synthesize factor(s) that induce RANKL expression in the fibrous stroma adjacent to the bone surface, leading to osteoclastic bone resorption.

In the present study, we examined the expression profiles of IL-6 and PTHrP in human OSCCs extensively and investigated the roles of IL-6 and PTHrP in osteoclast formation using various cancer cell lines. Herein we demonstrate that OSCC provides a suitable microenvironment for bone resorption not only by releasing PTHrP and IL-6 but also by stimulating stromal cells to synthesize IL-6.

Materials and Methods

Antibodies Used

Rat anti-mouse IL-6 receptor neutralizing monoclonal antibody (MR16-1)[32] and mouse anti-human PTHrP neutralizing monoclonal antibody[33] were provided by Chugai Pharmaceutical Co. Ltd. (Tokyo, Japan). Mouse anti-human IL-6, rat anti-mouse IL-6 neutralizing monoclonal antibodies, and rat and mouse IgG_1 used as controls were purchased from R&D Systems (Minneapolis, MN). Mouse anti-human RANKL monoclonal antibody (Calbiochem, Darmstadt, Germany), goat anti-human, mouse, and rat RANKL polyclonal antibody (sc-7628, Santa Cruz Biotechnology, Inc., Santa Cruz, CA), mouse anti-human IL-6 monoclonal antibody (Novocastra, Newcastle, UK), goat anti-mouse and rat IL-6 polyclonal antibody (sc-1265; Santa Cruz Biotechnology, Inc.), rabbit anti-human vimentin monoclonal antibody (Epitomics, Burlingame, CA), and rabbit anti-human CD14 and CD20 monoclonal antibodies (Epitomics) were used for immunohistochemical analyses.

Laser Capture Microdissection and Microarray Analysis

Primary oral cancer specimens were obtained from 43 anonymous patients who had been treated at the Dental Hospital of Tokyo Medical and Dental University. All cancers were histopathologically diagnosed as OSCC. None of the patients had received chemo- or radiotherapy before the specimens had been obtained. Informed consent was obtained from all of patients, and all of the experimental procedures were approved by the university ethics committee. Cancer cells were isolated from all of the hematoxylin-stained sections by laser capture microdissection as described previously.[34] From 9 patients, oral epithelial tissue adjacent to the tumor was also isolated by laser capture microdissection to compare the expression levels in this tissue with those in cancer cells. Microarray analyses were conducted on the samples using the Human Genome U24133 Plus 2.0 array purchased from Affymetrix as described previously.[34] Of the 43 cases of OSCCs in this study, 30 had been analyzed by microarrays in our previous report.[34] The expression level of mRNA was determined by fluorescence intensity, which was the absolute value of fluorescence intensity in each case.

Histochemical and Immunohistochemical Staining

After fixation in 10% neutral buffered formalin, small blocks approximately 1.5 × 1.0 × 0.5 cm containing the interface of tumor and bone were dissected from 13 of the surgical cases. These specimens were decalcified in 10% EDTA at 4°C for 4 weeks and embedded in paraffin. For immunohistochemical staining, the sections were pretreated with microwave irradiation in 0.01 mol/L citric acid for 1 hour at 80°C for RANKL antibody or PBS containing 0.1 mg/ml trypsin (BD, Franklin Lakes, NJ) for 30 minutes at 37°C for IL-6 antibody. After quenching of endogenous peroxidase activity by incubation in 0.3% hydrogen peroxide solution for 20 minutes, the sections were incubated overnight at 4°C with mouse anti-human RANKL monoclonal antibody (1:50) or mouse anti-human IL-6 antibody (1:50). After washing with PBS, the sections were incubated with peroxidase-conjugated secondary antibody (EnVision + Dual Link System Peroxidase Kit, Dako Denmark A/S, Glostrup, Denmark) for 1 hour. Diaminobenzidine was used as a chromogen. The RANKL- and IL-6-positive fibroblastic cells present between the invading tumor nests and the bone resorption surface were counted using Scion Imaging Software.

For immunofluorescent antibody staining, the specimens were dual-stained with a mouse anti-human IL-6 antibody (1:50) and goat anti-human vimentin antibody (1:200), anti-human CD14 antibody (1:500), or CD20 antibody (1:100) as a primary antibody. Goat anti-mouse IgG Alexa Fluor 488 and goat anti-rabbit IgG Alexa Fluor 594 (Invitrogen, Carlsbad, CA) were used as secondary antibodies and sections were incubated overnight at 4°C. After immunofluorescent antibody staining, specimens were scanned by a confocal laser microscope (Pascal LSM5, Carl Zeiss GmbH, Jena, Germany) with excitation wave lengths of 488 and 543 nm. Acquired fluorescent images and differential interference contrast images were processed using LSM Image browser (Carl Zeiss GmbH).

For immunohistochemical staining in the xenograft experiments, we used goat anti-human, mouse, and rat RANKL polyclonal antibody (Santa Cruz Biotechnology, Inc.), goat anti-mouse and rat IL-6 polyclonal antibody (Santa Cruz Biotechnology, Inc.), and mouse anti-human IL-6 monoclonal antibody (Novocastra) as primary antibodies. As secondary antibodies, an Imm PRESS REAGENT KIT with anti-goat Ig (MP-7405, Vector Laboratories, Burlingame, CA) was used to detect immunoreaction with goat antibodies and a Histofine Mouse Stain Kit (414322, Nichirei Corporation, Tokyo, Japan) was applied to detect immunoreaction with mouse antibody.

Cell Culture

We used four human OSCC cell lines (BHY, Ca9-22 [Ca9], HSC3, and HO1-u-1 [HO1]). BHY and Ca9 are derived from human gingival SCC, HSC3 from SCC of tongue, and HO1 from SCC of the floor of the mouth. In addition, we used four cancer cell lines derived from nonoral regions (EBC1, MKN28, A549, and MCF7). EBC1 is derived from lung SCC, MKN28 from gastric adenocarcinoma, A549 from lung adenocarcinoma, and MCF7 from breast adenocarcinoma. All cell lines were maintained in Dulbecco's modified Eagle's medium containing 10% fetal bovine serum (FBS) (Sigma-Aldrich, St. Louis, MO), 50 units/ml penicillin G, and 50 mg/ml streptomycin. The stromal cell line ST2, derived from mouse bone marrow, was maintained in RPMI 1640 medium containing 10% FBS. Human bone marrow-derived mesenchymal stem cells were cultured in Dulbecco's modified Eagle's medium containing 10% FBS, 2 ng/ml basic fibroblast growth factor, and antibiotics.[35] BHY was provided by Dr. Masato Okamoto (TELLA Inc., Tokyo, Japan), and Ca9-22 and HSC3 were purchased from the Japanese Collection of Research Bioresources. HO1-u-1 and MCF7 were provided by the Cell Resource Center for Biomedical Research (Tohuku University, Miyagi, Japan). EBC1, MKN28, A549, ST2, and human mesenchymal stem cells were purchased from RIKEN BioResource Center (Tsukuba, Japan).

Preparation of Conditioned Medium from Cancer Cell Lines

All of the cancer cells were grown to confluence in 100-mm dishes in Dulbecco's modified Eagle's medium containing 10% FBS. After washing with PBS three times, they were cultured for an additional 48 hours in 4 ml of serum-free α-modified minimum essential medium. The collected culture supernatants were centrifuged at 1500 rpm for 5 minutes and filtered using a 0.22-μm filter unit. The media thus obtained were stored at −80°C and used as conditioned medium (CM). For all experiments, the CM was diluted with α-modified minimum essential medium in a 1:1 ratio (50%).

RT-PCR Analyses

Total RNA extracted from the cultured cells was reverse-transcribed into cDNA using a First-Strand cDNA Synthesis Kit for RT-PCR (Roche Diagnostics, Indianapolis, IN). The cDNA products were amplified by RT-PCR using gene-specific primers as shown in Table 1. The amplified products of human *PTHrP*, human *IL-6*, human *OPG*, and human *ACTB* were electrophoresed on 2% agarose gel and visualized under UV light illumination after staining ethidium bromide staining. The mRNA expression levels of human *RANKL*, mouse *Rankl*, mouse *Opg*, human *IL-6*, and mouse *Il-6* were quantified by real-time RT-PCR using a Light-Cycler System (Roche Diagnostics) and a Platinum SYBR Green qPCR SuperMix UDG kit (Invitrogen) with the specific primers as shown in Table 1. The relative expression level of each mRNA was normalized to the 18S rRNA expression level.

Osteoclast Formation

The osteoclast formation activity in the CM was assessed using an *in vitro* osteoclast formation assay.[36] We inocu-